Alfvén wave cascades in a tokamak

S. E. Sharapov, B. Alper, H. L. Berk, D. N. Borba, B. N. Breizman et al.

Citation: Phys. Plasmas **9**, 2027 (2002); doi: 10.1063/1.1448346
View online: http://dx.doi.org/10.1063/1.1448346
View Table of Contents: http://pop.aip.org/resource/1/PHPAEN/v9/i5
Published by the American Institute of Physics.

Related Articles

High-resolution charge exchange measurements at ASDEX Upgrade
Rev. Sci. Instrum. 83, 103501 (2012)

Temporal and spectral evolution of runaway electron bursts in TEXTOR disruptions
Phys. Plasmas 19, 092513 (2012)

1.5D quasilinear model and its application on beams interacting with Alfvén eigenmodes in DIII-D
Phys. Plasmas 19, 092511 (2012)

Modification of Δ′ by magnetic feedback and kinetic effects
Phys. Plasmas 19, 092510 (2012)

Effect of toroidal rotation on the geodesic acoustic mode in magnetohydrodynamics
Phys. Plasmas 19, 094502 (2012)

Additional information on Phys. Plasmas

Journal Homepage: http://pop.aip.org/
Journal Information: http://pop.aip.org/about/about_the_journal
Top downloads: http://pop.aip.org/features/most_downloaded
Information for Authors: http://pop.aip.org/authors

ADVERTISEMENT

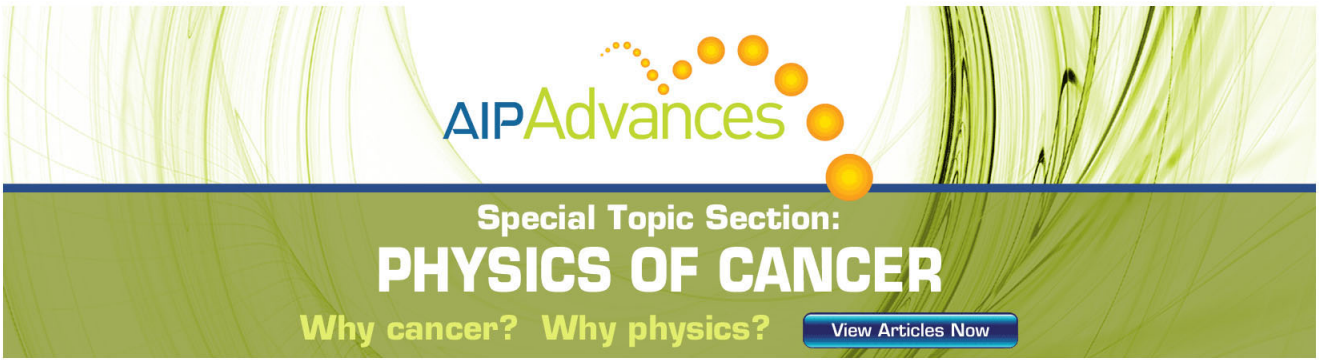

Downloaded 03 Oct 2012 to 194.81.223.66. Redistribution subject to AIP license or copyright; see http://pop.aip.org/about/rights_and_permissions

Alfvén wave cascades in a tokamak[a)]

S. E. Sharapov,[b)] B. Alper, H. L. Berk,[c)] D. N. Borba,[d)] B. N. Breizman,[c)] C. D. Challis, A. Fasoli,[e)] N. C. Hawkes, T. C. Hender, J. Mailloux, S. D. Pinches,[f)] D. Testa,[e)] and contributors to the EFDA–JET work programme[g)]
Euratom/UKAEA Fusion Association, Culham Science Centre, Abingdon, Oxfordshire OX14 3DB, United Kingdom

(Received 1 November 2001; accepted 10 December 2001)

Experiments designed for generating internal transport barriers in the plasmas of the Joint European Torus [JET, P. H. Rebut *et al.*, *Proceedings of the 10th International Conference, Plasma Physics and Controlled Nuclear Fusion, London* (International Atomic Energy Agency, Vienna, 1985), Vol. I, p. 11] reveal cascades of Alfvén perturbations with predominantly upward frequency sweeping. These experiments are characterized by a hollow plasma current profile, created by lower hybrid heating and current drive before the main heating power phase. The cascades are driven by ions accelerated with ion cyclotron resonance heating (ICRH). Each cascade consists of many modes with different toroidal mode numbers and different frequencies. The toroidal mode numbers vary from $n=1$ to $n=6$. The frequency starts from 20 to 90 kHz and increases up to the frequency range of toroidal Alfvén eigenmodes. In the framework of ideal magnetohydrodynamics (MHD) model, a close correlation is found between the time evolution of the Alfvén cascades and the evolution of the Alfvén continuum frequency at the point of zero magnetic shear. This correlation facilitates the study of the time evolution of both the Alfvén continuum and the safety factor, $q(r)$, at the point of zero magnetic shear and makes it possible to use Alfvén spectroscopy for studying $q(r)$. Modeling shows that the Alfvén cascade occurs when the Alfvén continuum frequency has a maximum at the zero shear point. Interpretation of the Alfvén cascades is given in terms of a novel-type of energetic particle mode localized at the point where $q(r)$ has a minimum. This interpretation explains the key experimental observations: simultaneous generation of many modes, preferred direction of frequency sweeping, and the absence of strong continuum damping. [DOI: 10.1063/1.1448346]

I. INTRODUCTION

Among the waves that exist in plasmas,[1] the shear Alfvén wave[2] constitutes one of the most significant modes of the magnetohydrodynamic (MHD) spectrum. Alfvén waves have been thoroughly investigated in magnetic fusion, where the problem of plasma heating by low frequency waves (see, e.g., a review Ref. 3 and references therein) and the problem of excitation of Alfvén instabilities by fusion-born α-particles[4,5] were the focus of both theory and experiment. An important aspect of the shear Alfvén waves in ideal MHD is the existence of a continuous spectrum,[6] which in a slab or cylindrical model takes the form

$$\omega_A^2(r)=k_\parallel^2(r)V_A^2(r). \tag{1}$$

These continuous waves are present when there are spatial inhomogeneities in Alfvén velocity, $V_A(r)=B_0/(4\pi\rho)^{1/2}$, and in the wave vector along the equilibrium magnetic field, $k_\parallel=\mathbf{k}\cdot\mathbf{B}_0/B_0$ (r is a radial coordinate across the magnetic field $\mathbf{B}_0$, and ρ is plasma mass density). For a wave of real frequency ω, either driven externally or excited by fast particles inside the plasma, Eq. (1) determines the position of a resonance layer, $r=r_{\rm res}$:

$$\omega=\omega_A(r_{\rm res}). \tag{2}$$

At that surface ideal MHD theory predicts absorption of wave energy by the plasma which is known as continuum damping.

It has been long recognized[4,7] that if the shear Alfvén continuous frequency as a function of radius has extremum points, $r=r_0$, satisfying

$$\left.\frac{d\omega_A(r)}{dr}\right|_{r=r_0}=0, \tag{3}$$

the Alfvén spectrum may contain discrete eigenvalues. Indeed in cylindrical geometry, when a combined effect of plasma current and inhomogeneous plasma density creates a minimum as a function of r in $\omega_A(r)$, a discrete MHD mode called the global Alfvén eigenmode (GAE)[7,8] has been found. The eigenfrequency of a GAE lies just below the minimum shear Alfvén frequency, $\omega_{\rm GAE}<\omega_A(r_0)$, so that

[a)]Paper BI1 6, Bull. Am. Phys. Soc. **46**, 21 (2001).
[b)]Invited speaker.
[c)]Institute for Fusion Studies, University of Texas, Austin, Texas.
[d)]EFDA-JET Close Support Unit & Euratom/IST Association, Lisbon, Portugal.
[e)]Plasma Science and Fusion Center, MIT, Cambridge, Massachusetts.
[f)]Max-Planck Institute für Plasmaphysik, Euratom Association, Garching, Germany.
[g)]See annex of J. Pamela *et al.*, "Overview of recent JET results and future perspectives," Fusion Energy, *Proceedings of the 18th International Conference On Fusion Energy, Sorrento, 2000* (IAEA, Vienna, 2001).

Downloaded 03 Oct 2012 to 194.81.223.66. Redistribution subject to AIP license or copyright; see http://pop.aip.org/about/rights_and_permissions

GAE frequency is slightly downshifted from the local Alfvén resonance condition (2) and thereby the GAE avoids strong continuum damping.

In toroidal geometry, toroidicity-induced gaps with the relevant extremum points determined by Eq. (3) are created within the shear Alfvén wave spectrum by toroidal coupling of different poloidal harmonics.[6,9] A discrete toroidicity-induced Alfvén eigenmode (TAE)[9] exists in this case, with TAE frequency within the gap. The toroidal generalization to condition (2) is not satisfied for frequencies in the TAE gap region, $\omega_A^{\min}(r_0)<\omega_{\mathrm{TAE}}<\omega_A^{\max}(r_0)$, and thus the TAE mode also does not experience strong continuum damping. However, a TAE mode may still be slightly damped, since it can interact with the shear Alfvén continuum in regions that are away from the region where the mode is principally localized.[10–12]

Beyond ideal MHD theory, the inclusion of finite ion Larmor radius and finite electron parallel conductivity effects create a kinetic Alfvén wave (KAW).[13] When finite ion Larmor radius effects are large enough, Eq. (2) transforms into the linear mode conversion condition, while Eq. (3) determines existence of potential wells for discrete standing KAWs,[4,14–16] which may exist in addition to the ideal MHD eigenmodes.

The presence of energetic particles in a plasma also can significantly alter its behavior from that predicted by ideal MHD. First, fast particles can perturbatively destabilize a basic MHD mode. Second, a sufficient number of fast particles can alter the very structure of the MHD spectrum (i.e., the energetic particles produce discrete modes that do not exist in their absence). This latter behavior is relevant to a shear Alfvén perturbation called an energetic particle mode (EPM).[17–21]

Experimentally, discrete weakly damped Alfvén eigenmodes are commonly observed in most tokamaks with fast particles generated by neutral beam injection (NBI),[22–24] ion-cyclotron resonance heating (ICRH),[25–27] and fusion reactions.[28] Significant progress in interpretation of the experimental data by the theory was achieved during recent years.[29]

The aim of this paper is to present both the experimental observations and the theoretical interpretation of a new type of Alfvén eigenmode that differs somewhat from the Alfvén modes discussed above. This mode is excited by ICRH-accelerated energetic ions in tokamaks that have nonmonotonic profiles of the safety factor $q(r)$, and the minimum value of $q(r)$, $q_{\min}$, evolves significantly in time. This Alfvén phenomenon, which we call an Alfvén wave cascade (AC), was first observed in JT-60U[30] negative magnetic shear experiments, and has been detected in many Joint European Torus (JET) discharges of a similar type.[31] These Alfvén perturbations exhibit upward frequency sweeping, with frequency starting at a frequency well below the TAE gap frequency and increasing up to the TAE frequency range.[30,31] In the framework of the ideal MHD model, a close correlation has been found in Refs. 31 and 32 between the time evolution of the Alfvén cascades and the evolution of the Alfvén continuum frequency (1) at the point of zero magnetic shear. The importance of the local extremum points of the Alfvén continuum (3) is therefore the focus of this paper.

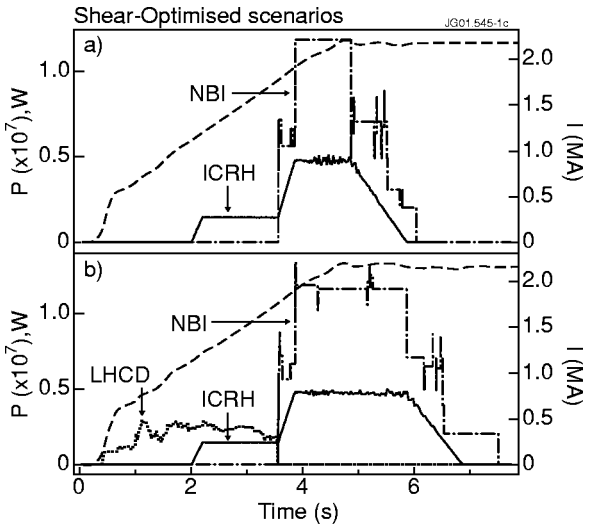

FIG. 1. Two similar JET discharges [pulses #49384 (a) and #49382 (b) with toroidal magnetic field $B_T=2.6$ T and plasma current $I_P^{\max}=2.2$ MA] with the only difference in 2.5 MW of LHCD applied at the preheating phase in #49382. In both discharges current shown by broken line was increasing from $I_P=1.1$ MA at $t=2$ s to $I_P=2.2$ MA at $t=5$ s.

Experimental conditions typical of JET plasmas and the experimental data for the ACs are presented in Sec. II. In Sec. III we analyze the Alfvén spectrum within the MHD framework and investigate orbits of ICRH-accelerated fast ions for JET equilibrium with hollow current profiles. Interpretation of the ACs within a model that combines the reduced MHD description of the shear Alfvén waves with drift kinetic description of the fast ions is presented in Sec. IV. MHD spectroscopy allowing a determination of evolution of the safety factor from ACs is presented in Sec. V. Conclusions are given in Sec. VI.

II. OBSERVATION OF ALFVÉN CASCADES IN JET PLASMAS

A. Experimental conditions

In JET, as in many other tokamaks, for particular current profiles, the plasma confinement improves spontaneously as the heating power exceeds a certain threshold value, and an internal transport barrier (ITB) forms in the plasma interior.[33] Important record parameters have been achieved in JET plasmas with ITBs. In particular, the JET record in deuterium plasma fusion performance, i.e., $S_n\approx 5.6\times 10^{16}\ \mathrm{s}^{-1}$ was achieved in ITB discharge[34] (pulse #40554). In deuterium–tritium (DT) plasma with ITB, the JET record ion temperature, $T_i(0)\approx 40$ keV, the ion temperature and pressure radial gradients, ≈ 150 keV/m and $\approx 10^6$ Pa/m (pulse #42940) were achieved.[33]

In order to trigger an ITB, additional heating is usually applied early in the discharge before the plasma current has been fully penetrated, as shown in Fig. 1. The central safety factor in this case can be significantly above unity and the magnetic shear can be low or negative in the plasma core when the principal heating is initiated, as shown in Fig. 2. One of the important JET results was the observation that

Downloaded 03 Oct 2012 to 194.81.223.66. Redistribution subject to AIP license or copyright; see http://pop.aip.org/about/rights_and_permissions

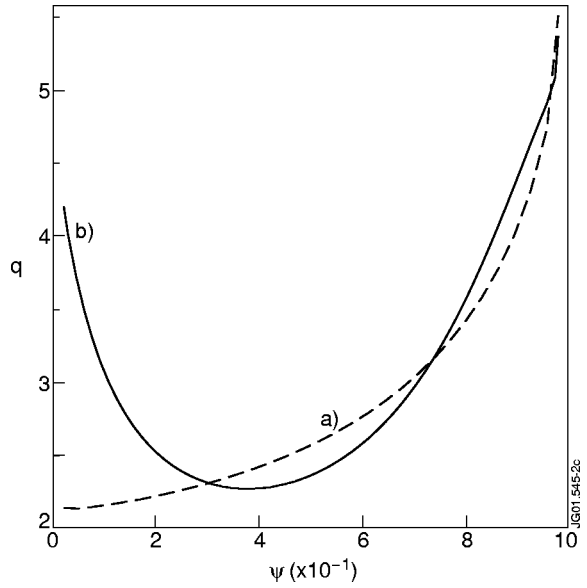

FIG. 2. Safety factor profiles $q(r)$ reconstructed by the EFIT code for (a) and (b) in Fig. 1. MSE measurements were used in EFIT for deeply reversed magnetic shear case #49382.

ITBs delivering high fusion performance enhancement were obtained with lower additional power following a lower-hybrid current drive (LHCD) prelude.[35,36] Although negative-shear ITBs differ from the ITBs obtained with monotonic $q(r)$ profiles[33] in many respects, they still exhibit improved transport properties and are easier to study experimentally due to the lower power threshold and higher resilience with respect to MHD perturbations.

Alfvén wave cascades are observed during the current ramp-up phase in nearly all JET plasmas when ICRH and LHCD power is applied in order to create a nonmonotonic $q(r)$ profile for subsequent triggering of an ITB.

B. Measurements of ACs with external magnetic coils

The measurements of Alfvén waves are performed on JET using a toroidal set of high-resolution magnetic pick-up coils connected to an analog to digital converter with a sampling rate of 1 MHz.[37] Magnetic fluctuation data, $\partial(\delta B_P)/\partial t$, are recorded with 12 bit resolution for 4 s during JET discharges. This measurement allows to determine mode amplitude at the edge to an accuracy $|\delta B_P/B_0| \leqslant 10^{-8}$. A toroidal set of three coils allows the determination of toroidal mode numbers from $n=-17$ to $n=17$.

Figures 3(a) and 3(b) show magnetic fluctuation data measured by the magnetic pick-up coils in the Alfvén frequency range during the preheating phase of two discharges with the power and current wave forms shown in Fig. 1. A comparison of Figs. 3(a) and 3(b) reveals that the Alfvén instabilities are very different in the two discharges, although the only difference between the discharges is that low-power LHCD, $P_{\mathrm{LHCD}} \approx 2.5$ MW, is applied in discharge #49382. In the plasmas without LHCD (#49384) the $q(r)$ profile was monotonic and the ICRH-accelerated hydrogen minority ions excited TAEs, Fig. 3(a), whose frequency followed the increase of plasma current in time. The comparison discharge,

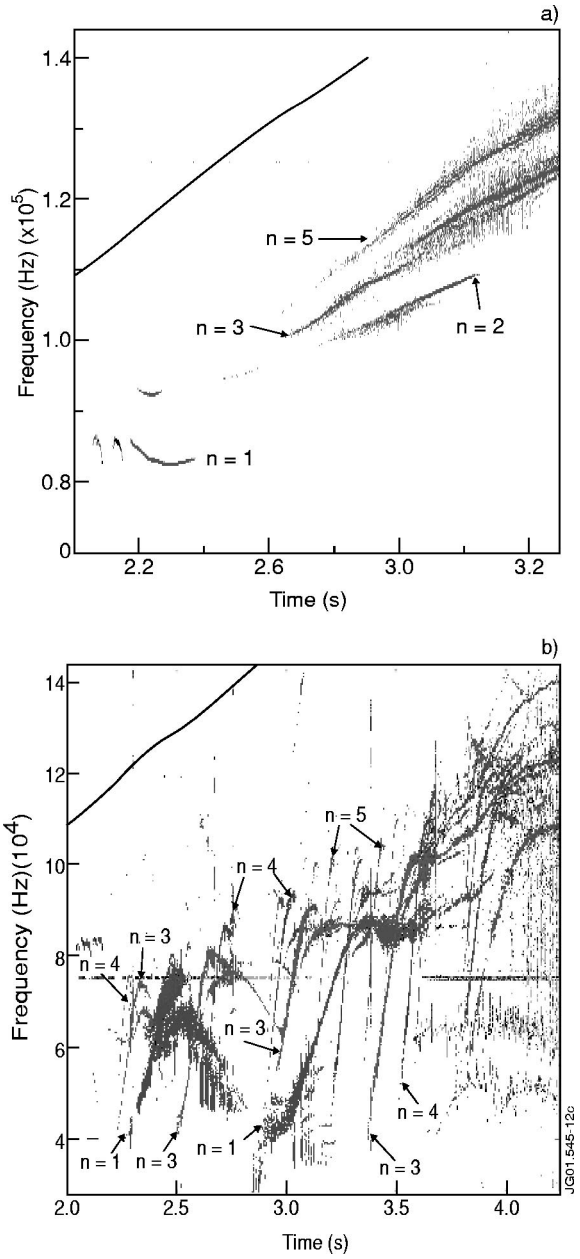

FIG. 3. (a) Spectrogram of the magnetic perturbations, measured by the external Mirnov coils in plasma with monotonic $q(r)$. Usual TAE modes are observed at frequencies $f_{\mathrm{TAE}} \cong 80-200$ kHz. Typically $\delta B_p \approx 10^{-6}$ T in the TAEs. Evolution of TAE frequency in time is caused by plasma current increase at the time of observation. (b) Spectrogram of the magnetic perturbations, measured by the external Mirnov coils in plasma with nonmonotonic $q(r)$. Alfvén cascades are observed at frequencies well below TAE frequency range, $f_{\mathrm{AC}} \cong 40-90$ kHz $\ll f_{\mathrm{TAE}}$. Typically $\delta B_p \approx 10^{-6}$ T in the cascades. Multiple branches of Alfvén cascades ranging from $n=1$ to $n=6$ are observed, with frequency sweeping proportional to the mode number. The trace is showing the slope of the plasma current increase.

in which LHCD created a nonmonotonic $q(r)$ profile shown in Fig. 2, exhibits Alfvén cascade (ACs) phenomena with the frequency sweeping below the TAE frequency, shown in Fig. 3(b). The toroidal mode numbers do not change for each branch of the perturbation as the relevant mode frequencies sweep upward.

ACs are observed in discharges similar to the pulse #49382 even after LHCD is switched off. This shows that

Downloaded 03 Oct 2012 to 194.81.223.66. Redistribution subject to AIP license or copyright; see http://pop.aip.org/about/rights_and_permissions

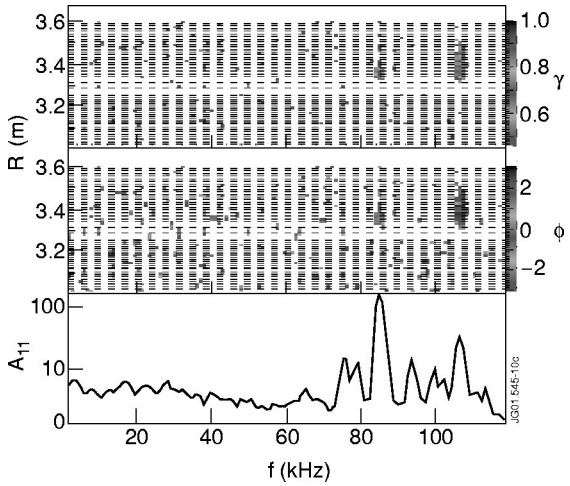

FIG. 4. Cross-correlation spectrogram for the amplitude γ and the phase ϕ of an Alfvén cascade. The radial location of the perturbation at $R \approx 3.4$ m (which corresponds to $r/a \approx 0.4$) is inferred from the cross-correlation between the external magnetics and the 48-channel electron cyclotron emission (ECE) diagnostic.

ACs are associated with nonmonotonic $q(r)$ profiles created by LHCD, rather than with LHCD itself. At the same time, since no ACs were observed without ICRH, we conclude that ICRH-accelerated ion tail is essential for ACs.

Each AC in Fig. 3(b) has pronounced upward frequency sweeping and consists of many modes with different toroidal mode numbers and different frequencies. The toroidal mode numbers vary from $n=1$ to $n=6$. The frequency of the Alfvén cascades starts from 40 to 90 kHz, well below the TAE frequency. During the cascade evolution, the frequency increases up to the frequency of the TAE gap. The rate of increase in the Alfvén cascade frequency is proportional to the mode number *n*. In addition, modes of different *n* occur at different times. For each branch of the AC, the frequency changes on a time scale $\tau \cong 0.1-0.5$ s, which is significantly longer than the time scale observed for other ''frequency-chirping'' modes on JET.[38] On the other hand, the time scale of the frequency change is of the order of the current increase time scale shown in Fig. 3(b). Therefore the temporal evolution of plasma equilibrium, and especially that of plasma current and $q(r)$ profile are important in determining frequency variation of ACs.

C. Internal measurements of Alfvén wave cascades

In some JET discharges with high ICRH power, internal plasma measurements with the electron cyclotron emission (ECE) and soft x-ray (SXR) diagnostics were also available for diagnosing ACs. An example of such measurements is shown in Fig. 4 for JET plasmas with nonmonotonic $q(r)$ at ICRH power in excess of 7 MW (pulse #53494). This level of ICRH power is much higher than the ~2 MW power threshold needed to excite the Alfvén cascades. For two branches of ACs observed at 85 kHz and 110 kHz, the cross-correlation analysis between the perturbed electron temperature, δT_e, and the magnetic perturbations, $\delta B_{\rm pol}$, is performed as shown in Fig. 4. The perturbed electron temperature is measured by a 48-channel ECE diagnostics with radially separated lines-of-sight, so that the radial mode structure in the plasma core is determined. The two pictures on the top of Fig. 4 show the amplitude and phase of the cross-correlation integral $I(r)$,

$$I(r) \propto \int \frac{\delta B_p \cdot \delta T_e(r)}{|\delta B_p| \cdot |\delta T_e(r)|} dt, \tag{4}$$

where the minor radius r is different for the different ECE channels and the time interval for the integration is 0.2 s. From Fig. 4 one can estimate the mode location on the low-field side of the torus as seen from the top. The two modes of the Alfvén cascade, $n=3$ at $f \cong 85$ kHz and $n=6$ at $f \cong 110$ kHz, are localized at major radius, ~3.4 m (the magnetic axis is at 2.97 m at that time), corresponding to $r/a \approx 0.4$. Note that modes of significantly different frequencies and mode numbers *n* are localized at nearly the same radial position.

A similar technique of cross-correlation between soft x-ray (SXR) measurements (which also depend on electron temperature perturbation, δT_e) and magnetic perturbation, $\delta B_{\rm pol}$ gives an estimate of localization of the perturbation in vertical direction. It is found that the mode at $f \cong 85$ kHz has localization peaks at a vertical minor radius of ~60 cm.

The measurements were repeated in this discharge 1 s later. For the branches of the Alfvén cascades seen at that time, $n=2$, 3, and 4 at $f \cong 70$ kHz, $f \cong 95$ kHz, and $f \cong 120$ kHz correspondingly, both the ECE and the x-ray measurements show that the mode localization is very close to the AC region seen in Fig. 4 at earlier time.

We conclude therefore that two important features are characteristic of ACs: (a) the mode localization region at about $r/a \approx 0.4$ is independent of the mode number, (b) the mode localization does not change significantly on a time scale of ≈1 s.

III. ALFVÉN SPECTRUM AND FAST IONS IN PLASMAS WITH HOLLOW CURRENT PROFILE

The analysis of the ACs above shows the existence of a region at around mid-radius of the tokamak, in which ACs are localized independently of their mode numbers. On the other hand, the Alfvén cascades are only observed in discharges with nonmonotonic $q(r)$ profile. In these discharges the zero magnetic shear point [where the $q(r)$ profile has a minimum] measured by the motional stark effect (MSE) diagnostics[39] also typically occurs at mid-radius. Thus, an investigation of Alfvén waves associated with the region surrounding the zero magnetic shear point, as well as study of the temporal evolution of the key equilibrium parameters in this region, is necessary for interpreting ACs.

A. Evolution of Alfvén continuous spectrum and the evolution of $q(r)$ profile

We start by investigating the Alfvén continuous spectrum as a function of radius and time in the framework of the ideal MHD model with an expectation that ACs basically trace the Alfvén continuum similarly to other types of Alfvén eigenmodes discussed in the Introduction. We calculate the continuum with the CSCAS code,[40] which accounts for tor-

Downloaded 03 Oct 2012 to 194.81.223.66. Redistribution subject to AIP license or copyright; see http://pop.aip.org/about/rights_and_permissions

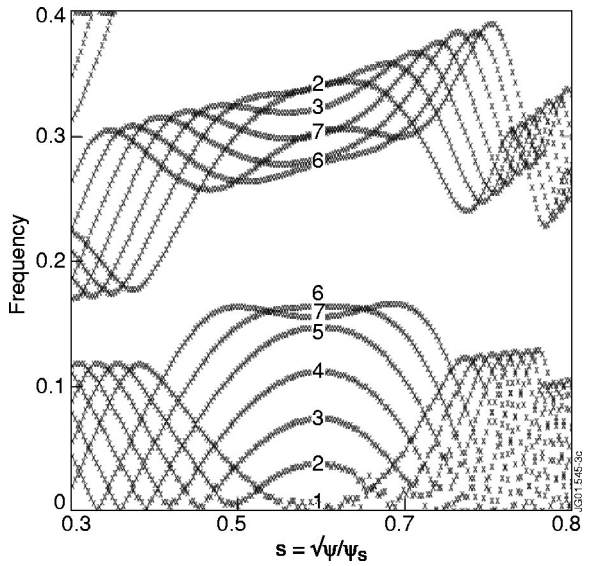

FIG. 5. The ideal MHD CSCAS code: normalized frequency $\omega R_0/V_A(0)$ of $n=1$ Alfvén continuous spectrum as a function of radius $s=(\psi_P/\psi_P^{\text{edge}})^{1/2}$ for several different values $q_{\min}$ associated with the evolution of $q_{\min}(t)$ from $q_{\min}=3$ down to $q_{\min}=2.4$ in reversed shear JET discharge. The sequence of the Alfvén continuum tips corresponding to values $q_{\min}=3,2.9,2.8,\ldots,2.4$ is shown by numbers 1,...,7.

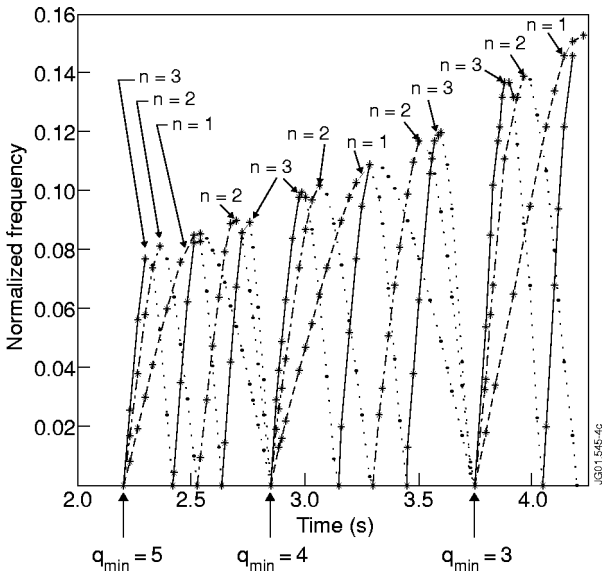

FIG. 6. The CSCAS analysis showing temporal evolution of the normalized frequency $\omega_A(r_{\min})R_0/V_A$ at $q=q_{\min}$ as $q_{\min}(t)$ decreases in time. Mode numbers plotted are $n=1$, $n=2$, and $n=3$. Solid lines indicate times of local maximum of the Alfvén continuum, while broken lines indicate times of local minimum of the Alfvén continuum.

oidal geometry. The temporal evolution of the Alfvén continuum frequency at the point of zero magnetic shear at $q_{\min}$ (''tip'' of the Alfvén continuum) is of major interest. In a ''cylindrical'' limit, this evolution is described by

$$\omega_A(r=r_{\min},t)=|k_{\parallel m}(t)|\cdot V_A(t), \tag{5}$$

with

$$k_{\parallel m}(t)=\frac{1}{R_0}\left(n-\frac{m}{q_{\min}(t)}\right),$$

where $r_{\min}$ is the zero magnetic shear point, and $q_{\min}(t)$ and $V_A(t)$ vary in time in accordance with the experiment. This behavior is quite similar to what emerges from the CSCAS code except that the numerical code automatically switches the dominant m number as the frequency approaches the TAE gap frequency.

Figure 5 shows the evolution from the CSCAS code of the value $\omega_A(t)$ for $n=1$ as $q_{\min}(t)$ gradually decreases from 3 down to 2.4. During the entire evolution the Alfvén continuum frequency as a function of radius has a local extremum determined by (3) that is very close to the point of zero magnetic shear, $q_{\min}$. During most of this time evolution the Alfvén continuum has a local *maximum* at $q_{\min}$ except when $q_{\min}$ approaches $q_{\min}=2.4$ (labeled 7). At low frequency, this local maximum of the frequency linearly increases as $q_{\min}$ decreases, but as the maximum frequency approaches the TAE gap, the local maximum changes to local minimum of the Alfvén continuum at $q_{\min}$ (marker 7 in Fig. 5). During the subsequent decrease of $q_{\min}$, this minimum of the Alfvén continuum decreases down to zero frequency, as the rational magnetic surface is formed at $q_{\min}=2$.

On a longer time scale, the evolution of the $n=1$ Alfvén continuum frequency as a function of $q_{\min}$ is shown in Fig. 6. The rate at which the Alfvén continuum tip passes zero frequency is determined by the rate of plasma current increase and diffusion. The highest frequency achieved by the local maximum of the Alfvén continuum is bounded by the frequency of the TAE gap. Since the frequency of TAE gap is inversely proportional to $q_{\min}$, the envelope of the highest frequencies is roughly proportional to the plasma current increase during the time of observation. If now we consider the temporal evolution of the Alfvén continuum frequency at $q_{\min}$ for $n=2$ and $n=3$ we observe a similar characteristic pattern of the intermittent maximum and minimum of Alfvén continuum at decreasing $q_{\min}$. However, the rate of the frequency sweeping and the repetition rate for the higher mode numbers are higher than for $n=1$, e.g., the $n=2$ mode frequency sweeps approximately twice as fast and this mode passes zero frequency not only at integer values of $q_{\min}$, but at half-integer values as well.

A comparison of the experimental data shown in Fig. 3(b) and the CSCAS modeling in Fig. 6 suggests that the following formula describes the frequency sweeping of the Alfvén cascades:

$$\omega(t)=\left|\frac{m}{q_{\min}(t)}-n\right|\cdot\frac{V_A}{R_0}+\Delta\omega, \tag{6}$$

where $\Delta\omega$ is an off-set frequency, possibly determined by Doppler shift in toroidally rotating plasma, by toroidal coupling corrections of the Alfvén continuum, and by fast ions.

The correspondence between the temporal evolution of the Alfvén continuum tip and the experimentally observed data suggests that ACs are similar to global Alfvén eigenmodes, whose frequency is close to where the localized shear Alfvén wave has an extremum as a function of radius determined by Eq. (3). However, in the standard theory of the global Alfvén eigenmode,[7,8] in cylindrical geometry, the extremum of the local Alfvén wave is a minimum, where n

Downloaded 03 Oct 2012 to 194.81.223.66. Redistribution subject to AIP license or copyright; see http://pop.aip.org/about/rights_and_permissions

$>m/q_{\min}(t)$. We see however that in order to explain the data we need the extremum Alfvén frequency to be a *maximum*, where $n<m/q_{\min}(t)$, in contrast to the GAE.[7,8]

B. Search for Alfvén eigenmodes associated with local maximum of Alfvén continuum

In order to investigate whether toroidal effects may significantly change the requirement for the existence of a ''cylindrical'' GAE, a numerical analysis of the Alfvén spectrum was performed with the antenna CASTOR[41] code in full toroidal JET geometry with nonmonotonic $q(r)$ profile. It was found[42] that a highly localized Alfvén eigenmode associated with the *maximum* of the Alfvén continuum could indeed exist in MHD framework. The eigenfrequency of this mode is just above the Alfvén continuum at the local maximum. However, this mode was found to exist only in the frequency range close to the TAE gap.[42] A similar mode was reported also in Ref. 43. However, since the experimentally observed frequencies of ACs start well below TAE frequency range, in contrast to the modes in Refs. 42 and 43, a search for additional modes was continued.

In this analysis, we have found that the addition of the finite Larmor radius and electron pressure in the parallel Ohms law that cause the kinetic Alfvén connection to the Alfvén wave does not help to establish the mode with upward frequency sweeping. The reason follows from the WKB dispersion relation for KAW,[13]

$$\alpha k_{\perp}^2 \rho_i^2 \omega^2 = \omega^2 - k_{\parallel}^2 V_A^2, \tag{7}$$

where ρ_i is the ion Larmor radius and

$$\alpha = \left(\frac{T_e}{T_i} + \frac{3}{4} \right).$$

In order to obtain a localized mode, we require $k_r^2<0$ far enough from $r=r_{\min}$ in either direction. Using Eq. (7) we see, as we move away from the mode center, that

$$\alpha k_r^2 \rho_i^2 \omega^2 = -\frac{V_A^2}{R^2} \frac{m q_{\min}''}{q_{\min}^2} (r-r_{\min})^2 \left(n - \frac{m}{q_{\min}} \right). \tag{8}$$

Thus, for $q_{\min}''>0$, mode localization requires $n>m/q_{\min}$, a result that is not compatible with the experiment.

C. ICRH-accelerated ions in JET plasmas with hollow current profile

Since neither the MHD model, nor the thermal ion finite Larmor radius effects explain the ACs, we now consider a possible new energetic particle mode, associated with hot ICRH-accelerated ions and the existence of nonmonotonic $q(r)$ profile. We first use the HAGIS[44] and CASTOR-K[45] codes in order to investigate the orbits of ICRH-accelerated hydrogen minority ions in JET plasmas with hollow current profiles. Fast ion distribution function resulting from on-axis ICRH heating is peaked about a pitch-angle given by

$$\Lambda = \frac{\mu B_0}{E} = 1. \tag{9}$$

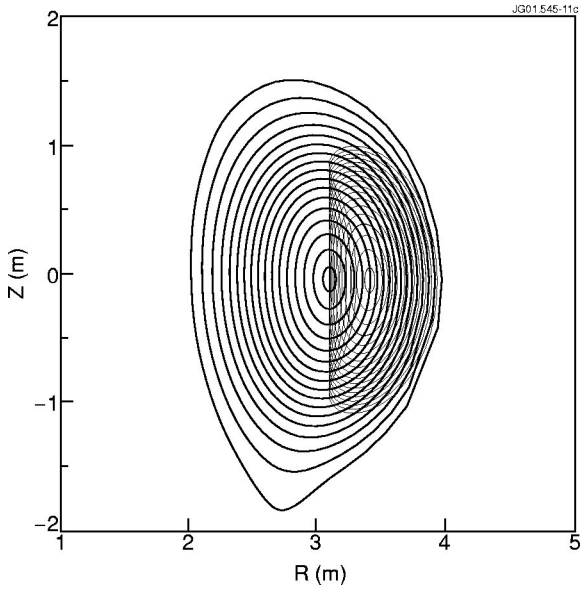

FIG. 7. The HAGIS code analysis of the orbits of ICRH-accelerated hydrogen minority ions in JET equilibrium (pulse #49382) with deeply reversed magnetic shear, $q_{\min}=3.95$, $q(0)=8.5$. Twenty particle orbits are launched between radii corresponding to the normalized poloidal magnetic fluxes $\psi=0.01$ and $\psi=0.99$ at the outboard mid-plane, $\vartheta=0$. All the energetic ions have energy 500 keV and the pitch-angle calculated such that $\Lambda=\mu B_0/E=1$.

This distribution function consists of trapped particles with bounce points, $V_{\parallel}=0$, at the B contour through the magnetic axis, $B=B_0$, and of passing ions with potato orbits,[46] for which $V_{\parallel}$ does not change sign. In order to estimate the proportion between the banana and potato orbits in typical discharges with ICRH, an equilibrium was investigated with a deeply reversed magnetic shear (pulse #49382). The fast ions were launched on the outboard mid-plane with $\Lambda=1$. The trajectories of particles launched at the same energy 500 keV are shown in Fig. 7. For the potato orbits that never bounce, $\dot{\phi}>0$, one finds that the average toroidal drift frequency $\overline{\dot{\phi}} \equiv \omega_{Dh}$ is larger than the poloidal (bounce/transit) frequency ω_{bh}. When we investigate energetic ions of somewhat different energy at different radial positions, we find that almost all ions within $q_{\min}$ have orbits of the potato type, with an average toroidal drift frequency [Fig. 8(a)] larger than ω_{bh} [Fig. 8(b)]. This inequality would be the opposite for the same pitch angle at lower energy where the particle would have a standard banana orbit. In addition the average toroidal drift frequencies are also larger than the frequency of ACs. In kinetic theory one can show that a major simplification arises if

$$\omega \leqslant \omega_{bh} \ll n \omega_{Dh} \tag{10}$$

is marginally satisfied for $n=1$, and even better for higher toroidal mode numbers. Thus, the ordering given by Eq. (10) will be used in the kinetic description of ICRH-accelerated fast ions.

IV. INTERPRETATION OF ALFVÉN CASCADES

We now search for an energetic particle mode associated with nonmonotonic $q(r)$ profiles and potato orbits of ICRH-

Downloaded 03 Oct 2012 to 194.81.223.66. Redistribution subject to AIP license or copyright; see http://pop.aip.org/about/rights_and_permissions

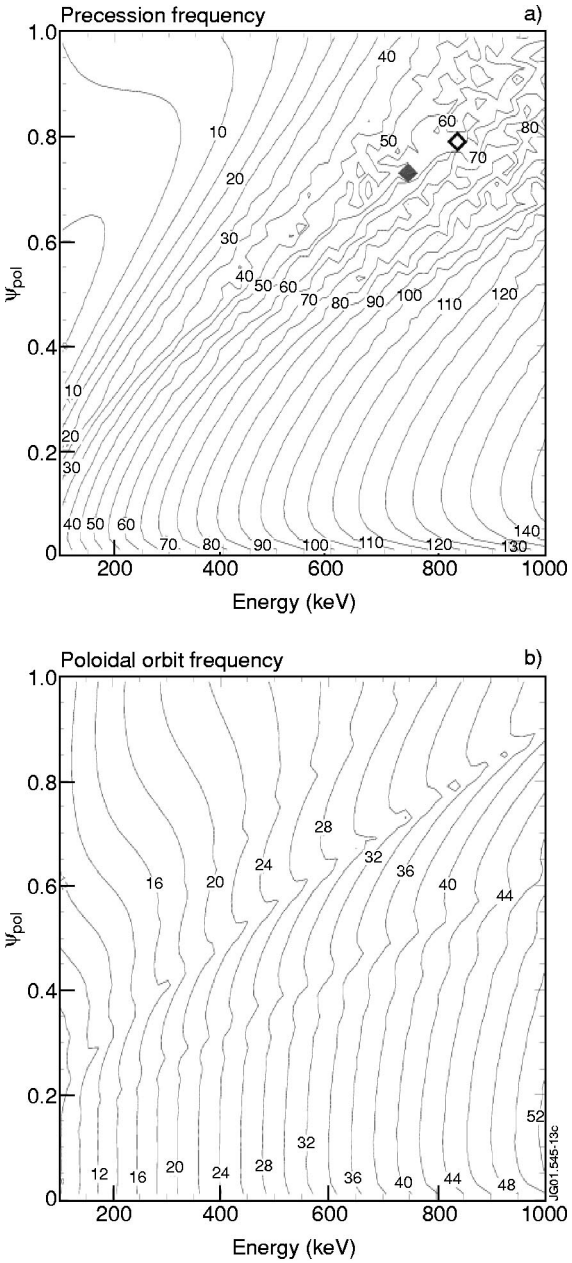

FIG. 8. (a) Variation of toroidal drift frequency, $\langle \dot{\phi} \rangle$, with launch energy and radius (normalized poloidal flux) for particles with $\Lambda = 1$. (b) Variation of orbit frequency (transit/bounce frequency), with launch energy and radius (normalized poloidal flux) for particles with $\Lambda = 1$.

accelerated ions. The mode description is based on a reduced MHD model of shear Alfvén perturbations and the drift kinetic model of energetic particles.[32] In a low-beta plasma in a large-aspect-ratio torus, the perturbed vector potential of the shear Alfvén wave can be represented by a single scalar function, $\delta\Phi$, as follows:

$$\delta \mathbf{A} = \nabla \delta\Phi - \frac{\mathbf{B}}{B^2}(\mathbf{B}\cdot\nabla\delta\Phi),$$

where $\mathbf{B}$ is the equilibrium magnetic field, with the perturbed electric and magnetic fields given by

$$\delta \mathbf{E} = -\frac{1}{c}\frac{\partial \delta \mathbf{A}}{\partial t}, \quad \delta \mathbf{B} = \nabla \times \delta \mathbf{A},$$

and the symbol δ is used to represent a linearly perturbed quantity. By using the charge neutrality condition, $\mathrm{div}\,\mathbf{j} = 0$ with the perturbed perpendicular current, $\delta \mathbf{j}_\perp \equiv \delta \mathbf{j} - \mathbf{B}(\mathbf{B}\cdot\delta\mathbf{j})/B^2$, calculated from the momentum balance equation, the derivation procedure of Ref. 32 gives

$$\nabla \cdot \frac{1}{V_A^2 B^2}[\mathbf{B}\times[\nabla \delta\ddot{\Phi}\times\mathbf{B}]] = (\mathbf{B}\cdot\nabla)\frac{1}{B^2}\nabla\cdot\left[\mathbf{B}\times\left[\nabla\left(\frac{\mathbf{1}}{B^2}(\mathbf{B}\cdot\nabla\delta\Phi)\right)\times\mathbf{B}\right]\right] - \left(\nabla\left(\frac{1}{B^2}(\mathbf{B}\cdot\nabla\delta\Phi)\right)\cdot\boldsymbol{\Delta}\mathbf{B}\right) - \nabla\cdot\frac{4\pi}{B^2}[\mathbf{B}\times\delta\mathbf{F}]. \quad (11)$$

The term

$$\delta F_\alpha \equiv -\delta\frac{\partial}{\partial x_\beta}\left[P_\perp\left(\delta_{\alpha\beta} - \frac{B_\alpha B_\beta}{B^2}\right) + P_\parallel \frac{B_\alpha B_\beta}{B^2}\right] \quad (12)$$

represents the force from the perturbed anisotropic pressure, which is dominated by the fast ions and can be calculated with the use of the kinetic guiding center theory. A relation found in Ref. 47,

$$-\nabla\cdot\frac{1}{B^2}[\mathbf{B}\times\delta\mathbf{F}] = \frac{e}{4\pi c}\int d^3\nu(\mathbf{v}_D\cdot\nabla\delta f), \quad (13)$$

simplifies the derivation significantly in the limit of inequality given by Eq. (10). Here e is the energetic particle charge, $\mathbf{v}_D$ is the magnetic field gradient and curvature drift velocity, and the gradient ∇ operates on the perturbed distribution function δf with energy w and magnetic moment μ held fixed. In order to evaluate the right-hand side of Eq. (13) we use the linearized drift kinetic equation

$$\frac{\partial \delta f}{\partial t} + \nu_\parallel \mathbf{b}\cdot\nabla\delta f + \mathbf{v}_D\cdot\nabla\delta f + [\delta(\nu_\parallel\mathbf{b})]\cdot\nabla f + (\delta\mathbf{v}_D)\cdot\nabla f + \mathbf{v}_{E\times B}\cdot\nabla f + \frac{\nu_\parallel}{\Omega}\left[\mathbf{b}\times\frac{\partial\delta\mathbf{b}}{\partial t}\right]\cdot\nabla f + \left[\mu\frac{\partial\delta B}{\partial t} + e(\nu_\parallel\mathbf{b}\cdot\delta\mathbf{E} + \mathbf{v}_D\cdot\delta\mathbf{E})\right]\frac{\partial f}{\partial w} = 0 \quad (14)$$

with

$$w \equiv \frac{m\nu_\parallel^2}{2} + \mu B, \quad \mathbf{v}_D \equiv \frac{1}{\Omega}\mathbf{b}\times\left(\frac{\mu}{m}\nabla B + \nu_\parallel^2(\mathbf{b}\cdot\nabla)\mathbf{b}\right),$$

$$\mathbf{v}_{E\times B} \equiv \frac{c}{B^2}[\delta\mathbf{E}\times\mathbf{B}], \quad (15)$$

where Ω is the fast particle gyrofrequency. Note that the integrand in Eq. (14) is exactly the third term on the left-

Downloaded 03 Oct 2012 to 194.81.223.66. Redistribution subject to AIP license or copyright; see http://pop.aip.org/about/rights_and_permissions

hand side of Eq. (13). Using Eq. (10) we see that the third term in Eq. (14) is the only term involving δf that we need to retain for low frequency modes with large mode numbers. Then Eq. (13) can be expressed in terms of the local field amplitudes

$$\nabla\cdot\frac{1}{B^2}[\mathbf{B}\times\delta\mathbf{F}]=\frac{e}{4\pi B}[\delta\mathbf{E}\times\mathbf{B}]\cdot\nabla\frac{\int f\,d^3\nu}{B}+\frac{e}{4\pi c}\delta\mathbf{B}\cdot\nabla\frac{\int\nu_\parallel f\,d^3\nu}{B}-\frac{e}{4\pi B^2}\times\{[\delta\mathbf{E}\times\mathbf{B}]\cdot(\mathbf{b}\cdot\nabla)\mathbf{b}\}\int f\,d^3\nu.$$

In contrast to earlier studied EPMs,[17–21] existence of which was determined by a nonlocal resonant contribution of energetic ions to the mode energy, the above expression describes a radially local term caused by energetic particles. The sign of the difference between toroidal drift frequency and the mode frequency is positive due to the large potato-type orbits.

In order to estimate the effect due to the presence of the fast ion population, we take into account that since the AC frequencies are well below the TAE frequency range, one can disregard the toroidal coupling effect and investigate a simplified ''cylindrical'' solution of Eq. (11) in the form

$$\delta\Phi=F(r)\exp(-i\omega t+in\varphi-im\theta),\tag{16}$$

where φ is the toroidal angle, and $F(r)$—the radial eigenfunction. A straightforward averaging procedure with the assumptions of $m\gg1$, and large aspect ratio equilibrium with circular flux surfaces, gives the following equation for $F(r)$:

$$\frac{m^2}{r^2}\left(\frac{\omega^2}{V_A^2}-k_\parallel^2\right)F-\frac{\partial}{\partial r}\left(\frac{\omega^2}{V_A^2}-k_\parallel^2\right)\frac{\partial F}{\partial r}=-\frac{4\pi e}{cB}\frac{m}{r}F\frac{\partial}{\partial r}\left[\omega\langle n_{\text{fast particles}}\rangle-k_\parallel\left\langle\frac{1}{e}j_{\parallel\text{fast particles}}\right\rangle\right].\tag{17}$$

The angular brackets in this equation denote flux surface averaging, and the terms in the right-hand side represent density and parallel current of the fast ions correspondingly. We expand the parallel wave number,

$$k_\parallel\equiv\frac{1}{R}\left(n-\frac{m}{q(r)}\right),$$

about the point $r=r_{\min}$ where $q=q_{\min}$ (the point of zero shear), and we look for a mode frequency close to, but above, the Alfvén continuum, $\delta\omega\equiv\omega-\omega_A$. We introduce a new dimensionless radial variable $x\equiv S^{1/2}(r-r_{\min})/r_{\min}$, and function $\Psi(x)=\psi(x)\cdot(S+x^2)^{1/2}$, where

$$S\equiv\frac{\omega^2-\omega_A^2}{\omega_A^2}\frac{mq_{\min}}{r_{\min}^2q''_{\min}}(m-nq_{\min}).$$

Then we can rewrite Eq. (17) as

$$S\Psi-\frac{\partial}{\partial x}\frac{\partial\Psi}{\partial x}=\Psi\frac{Q}{(1+x^2)}-\Psi\frac{1}{(1+x^2)^2},\tag{18}$$

where

$$Q\equiv-\frac{4\pi eRq_{\min}^2}{cB_0r_{\min}q''_{\min}}\frac{\partial}{\partial r}\left(\frac{V_A|m-nq_{\min}|}{(m-nq_{\min})}\langle n_h\rangle+\left\langle\frac{j_{\parallel h}}{e}\right\rangle\right).$$

Localized solutions exist for Eq. (18) if the parameter Q determined by the combination of the fast ion contribution and the slope of the potential well, q'', at the $q_{\min}$ location, exceeds a critical value[32]

$$Q>Q_{\text{crit}}=\tfrac{1}{4}.\tag{19}$$

It is important to note here that Q_{crit} does not depend on the mode number, and this result fits the experimental data, where modes of different mode numbers are observed simultaneously. Eigenvalues of the localized solutions are given by

$$S=Q-(2l+1)Q^{1/2}\quad\text{if}\quad Q\gg1,$$

$$S=\exp(-2l\pi/(Q-1/4)^{1/2})\quad\text{if}\quad Q-Q_{\text{crit}}\ll1.$$

Thus, we see that the ICRH-accelerated energetic ions with potato orbits can create a discrete spectrum of eigenmodes with frequencies just above the local maximum of Alfvén continuum.

V. MHD SPECTROSCOPY THROUGH DETECTING ALFVÉN WAVE CASCADES

In the present section we demonstrate possibility of MHD spectroscopy using the Alfvén wave cascades excited by ICRH-accelerated ions in JET plasmas with strongly nonmonotonic $q(r)$ profiles. The understanding of the physics of the Alfvén wave cascades allows determination of features of the $q(r)$ profile from the clustering of different toroidal mode number cascades in time.[31] This technique based on AC requires ICRH power only and may become an important complimentary tool for $q(r)$-profile measurements with the MSE diagnostics based on NBI.

Figure 9 shows the ACs observed during the ''preheat-

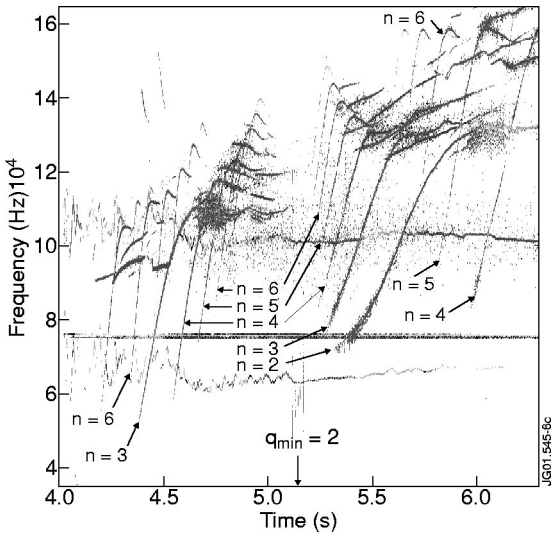

FIG. 9. Alfvén cascades observed in JET discharge with shear reversed equilibrium (pulse #53488). TAEs are observed in the frequency range 120–160 kHz at $t>5.3$ s.

Downloaded 03 Oct 2012 to 194.81.223.66. Redistribution subject to AIP license or copyright; see http://pop.aip.org/about/rights_and_permissions

TABLE I. Inferred $q_{\min}$ values for discharge #53488.

Time, s	4.3	4.5	4.6	4.65	5.2	5.6	5.7	5.9
n	3,6	4	5	6	2,3,4,5,6	6	5	4
$q_{\min}$	2.33	2.25	2.2	2.18	2	1.82	1.8	1.75

ing'' phase of a discharge with magnetic field 2.5 T and plasma current 2.2 MA (pulse #53488), which are excited by energetic ions accelerated by ICRH, $P_{\mathrm{ICRH}} \approx 4$ MW. The deeply reversed shear configuration was created by LHCD, $P_{\mathrm{LHCD}} \leqslant 2.7$ MW, applied during the time interval $t < 4.1$ s. During the time of observation, from $t=4$ s to $t=5.3$ s, the plasma current was increasing from 1.57 MA to 2.2 MA, due to a current ramp-up ≈ 0.3 MA/s, and the current wave form had a flat top 2.2 MA for $t > 5.3$ s. The safety factor was decreasing due to the increase of total plasma current and the current diffusion on a resistive time scale, determined by electron temperature evolution, with $T_e(0) \approx 4$ keV at $t=4$ s to $T_e(0) \approx 7.5$ keV at $t=6$ s. NBI power, $P_{\mathrm{NBI}} \approx 4$ MW, was applied at $t=4.5$ s. The electron density increased from $n_e(0) \approx 2 \times 10^{19}$ m^{-3} for $t=4$ s to $n_e(0) \approx 3 \times 10^{19}$ m^{-3} for $t=6$ s.

The toroidal mode numbers in the ACs vary from $n=2$ to $n=6$. The $n=4$ Alfvén cascade at $t \approx 5.9$ s has the poloidal mode numbers $m \approx 7-8$. The internal ECE measurements show that the Alfvén cascades are localized at $r/a \approx 0.4$, which is close to the point of zero magnetic shear as measured by the MSE diagnostics with NBI blip at somewhat earlier time, $t \approx 3.1$ s.

Considering Eq. (6) as a diagnostic tool for interpreting the Alfvén cascades in Fig. 9, one sees that, in accordance with Eq. (6), the modes of different n satisfy the condition $m - n q_{\min}(t) = 0$ at different times as $q_{\min}$ passes different sets of rational magnetic surfaces during the evolution. For example, the $n=1$ rational surfaces occur when $q_{\min}$ passes integer values 1, 2, 3,...; the $n=2$ rational surfaces occur when $q_{\min}$ passes integer and half-integer values 1, 3/2, 2, 5/2,...; $n=3$ rational surfaces occur when $q_{\min}$ passes 1, 1.33, 1.67, 2, 2.33,..., etc. Applying Eq. (6) to the pattern of cascades in Fig. 9, one explains the simultaneous excitation of Alfvén cascades with all toroidal mode numbers from $n=2$ to $n=6$ at $t \approx 5.2$ s as an example of $q_{\min}$ passing an integer value. From the MSE measurements at earlier time, $t \approx 3.1$ s, the value of $q_{\min}=2.8$ was found. Since $q_{\min}$ in this discharge does not pass 1 (no sawtooth associated with $q=1$ was observed in this discharge), and the evolution of $q_{\min}$ is a monotonically decreasing function of time, one concludes that $q_{\min}=2$ at $t \approx 5.2$ s. Considering ACs with higher toroidal mode numbers and using Eq. (6), we obtain Table I, which shows summary of the Alfvén cascades observations with the relevant values of $q_{\min}$ inferred from the toroidal mode number measurements.

We conclude that the use of Alfvén cascades for diagnostic purposes is a promising aspect of MHD spectroscopy. Future dedicated experiments must be performed with combined MSE measurements and MHD spectroscopy, in order to benchmark the results obtained from the MSE with the MHD spectroscopy.

VI. CONCLUSIONS

We have analyzed, both experimentally and theoretically, the Alfvén wave cascades, excited by ICRH-accelerated energetic ions in JET tokamak plasmas with nonmonotonic safety factor profiles. These cascades exhibit upward frequency sweeping, which is consistent with the evolution of Alfvén continuum at the point of zero magnetic shear, when the extremum of the Alfvén continuum is a maximum. This correlation facilitates the study of the time evolution of both the Alfvén continuum and the safety factor, $q(r)$, at the point of zero magnetic shear and makes it possible to use Alfvén cascades for inferring $q(r)$. An interpretation of the Alfvén cascades is given in terms of a novel-type of energetic particle mode localized at the point where $q(r)$ has a minimum. This type of EPM is determined by the reactive part of the response of the ions with the potato-type orbits inside $q_{\min}$, with the mean toroidal drift frequency larger than both poloidal orbit frequency and the mode frequency. This interpretation explains key experimental observations: simultaneous generation of many modes and a preferred direction of frequency sweeping.

The detailed understanding of the physics of the Alfvén wave cascades allows to determine of when a particular $q_{\min}$ enters the plasma. Moreover, in some cases ECE and SXR diagnostics allow the location of the cascade mode (and therefore of $q_{\min}$) to be determined as well. Thus, Alfvén cascades are very promising for use as an MHD spectroscopy diagnostic, building on the substantial understanding which has been achieved for these modes.

ACKNOWLEDGMENTS

The authors are grateful to Task Force S2 for conducting the shear-reversal experiments and to F. Zonca (ENEA/Euratom, Frascati) for important discussions.

This work has been partly performed under the framework of JET Joint Undertaking and partly under the European Fusion Development Agreement. It is partly funded by Euratom and the UK Department of Trade and Industry. The work of H.L.B. and B.N.B. was partly supported by the U.S. Department of Energy Contract No. DE-FG03-96ER-54346, and the work of A.F. and D.T. was partly supported by the U.S. Department of Energy Contract No. DE-F602-89ER-54563.

[1] T. H. Stix, *The Theory of Plasma Waves* (Advanced Physics Monograph Series, McGraw-Hill, New York, 1962), p. 1.
[2] H. Alfvén, Ark. Mat., Astron. Fys. **27A**, 1 (1940).
[3] J. Vaclavic and K. Appert, Nucl. Fusion **31**, 1945 (1991).
[4] M. N. Rosenbluth and P. H. Rutherford, Phys. Rev. Lett. **34**, 1428 (1975).
[5] A. B. Mikhailovskii, Sov. Phys. JETP **41**, 890 (1975).
[6] J. P. Goedbloed, Phys. Fluids **18**, 1258 (1975).
[7] K. Appert, R. Gruber, F. Troyon, and J. Vaclavic, Plasma Phys. Controlled Fusion **24**, 1147 (1982).
[8] D. W. Ross, G. L. Chen, and S. M. Mahajan, Phys. Fluids **25**, 652 (1982).
[9] C. Z. Cheng, L. Chen, and M. S. Chance, Ann. Phys. (N.Y.) **161**, 21 (1985).
[10] F. Zonca and L. Chen, Phys. Rev. Lett. **68**, 592 (1992).
[11] M. N. Rosenbluth, H. L. Berk, J. W. Van Dam, and D. M. Lindberg, Phys. Rev. Lett. **68**, 596 (1992).
[12] H. L. Berk, R. R. Mett, and D. M. Lindberg, Phys. Fluids B **5**, 3969 (1993).

Downloaded 03 Oct 2012 to 194.81.223.66. Redistribution subject to AIP license or copyright; see http://pop.aip.org/about/rights_and_permissions

[13]A. Hasegawa and L. Chen, Phys. Fluids **19**, 1924 (1976).
[14]R. R. Mett and S. M. Mahajan, Phys. Fluids B **4**, 2885 (1992).
[15]J. Candy and M. N. Rosenbluth, Phys. Plasmas **1**, 356 (1994).
[16]B. N. Breizman and S. E. Sharapov, Plasma Phys. Controlled Fusion **37**, 1057 (1995).
[17]S. T. Tsai and L. Chen, Phys. Fluids B **5**, 3284 (1993).
[18]L. Chen, Phys. Plasmas **1**, 1519 (1994).
[19]F. Zonca and L. Chen, Phys. Plasmas **3**, 323 (1996).
[20]C. Z. Cheng, N. N. Gorelenkov, and C. T. Hsu, Nucl. Fusion **35**, 1639 (1995).
[21]S. Bernabei, M. G. Bell, R. Budny *et al.*, Phys. Plasmas **6**, 1880 (1999).
[22]K. L. Wong, R. J. Fonck, S. F. Paul *et al.*, Phys. Rev. Lett. **66**, 1874 (1991).
[23]W. W. Heidbrink, Nucl. Fusion **31**, 1635 (1991).
[24]D. Borba, B. Alper, R. Budny, A. Fasoli, R. F. Heeter, W. Kerner, S. E. Sharapov, and P. Smeulders, Nucl. Fusion **40**, 775 (2000).
[25]K. L. Wong, J. R. Wilson, and Z. Y. Chang, Plasma Phys. Controlled Fusion **36**, 879 (1994).
[26]H. Kimura, M. Saigusa, M. Moriyama *et al.*, Phys. Lett. A **199**, 86 (1995).
[27]A. Fasoli, B. N. Breizman, D. Borba, R. F. Heeter, M. S. Pekker, and S. E. Sharapov, Phys. Rev. Lett. **81**, 5564 (1998).
[28]R. Nazikian, G. Y. Fu, S. H. Batha *et al.*, Phys. Rev. Lett. **78**, 2976 (1997).
[29]ITER Physics Basis, Chapter 5: Physics of energetic ions, Nucl. Fusion **39**, 2471 (1999).
[30]H. Kimura, Y. Kusama, M. Saigusa *et al.*, Nucl. Fusion **38**, 1303 (1998).
[31]S. E. Sharapov, D. Testa, B. Alper, D. N. Borba, A. Fasoli, N. C. Hawkes, R. F. Heeter, M. J. Mantsinen, and M. G. Von Hellermann, Phys. Lett. A **289**, 127 (2001).
[32]H. L. Berk, D. N. Borba, B. N. Breizman, S. D. Pinches, and S. E. Sharapov, Phys. Rev. Lett. **87**, 185002 (2001).
[33]C. Gormezano, Y. F. Baranov, C. D. Challis *et al.*, Phys. Rev. Lett. **80**, 5544 (1998).
[34]F. X. Soldner and The JET Team, Plasma Phys. Controlled Fusion **39**, B353 (1997).
[35]C. D. Challis, Y. F. Baranov, G. D. Conway *et al.*, Plasma Phys. Controlled Fusion **43**, 861 (2001).
[36]J. Mailloux, B. Alper, Y. Baranov *et al.*, Phys. Plasmas **9,** 2156 (2002).
[37]A. Fasoli, D. N. Borba, C. Gormezano *et al.*, Plasma Phys. Controlled Fusion **39**, B287 (1997).
[38]S. E. Sharapov, D. Borba, A. Fasoli, W. Kerner, L.-G. Eriksson, R. F. Heeter, G. Huysmans, and M. J. Mantsinen, Nucl. Fusion **39**, 373 (1999).
[39]N. Hawkes, B. C. Stratton, T. Tala *et al.*, Phys. Rev. Lett. **87**, 115001 (2001).
[40]S. Poedts and E. Schwartz, J. Comput. Phys. **105**, 165 (1993).
[41]G. T. A. Huysmans, W. Kerner, D. Borba, H. A. Holties, and J. P. Goedbloed, Phys. Plasmas **2**, 1605 (1995).
[42]D. Borba, H. L. Berk, B. N. Breizman, A. Fasoli, F. Nabais, S. D. Pinches, S. E. Sharapov, and D. Testa, ''Modeling of Alfvén waves in JET plasmas with the CASTOR-K code,'' 7th IAEA TCM on Energetic Particles, Gothenburg, Sweden, 9–11 October 2001, Nucl. Fusion (submitted).
[43]A. Fukuyama and T. Akutsy, ''Analysis of Alfvén eigenmodes driven by energetic ions in toroidal plasmas with weak or negative magnetic shear,'' *Proceedings of 7th IAEA TCM on Energetic Particles, Gothenburg, Sweden, 9–11 October 2001* (Chalmers University of Technology, Sweden, to be published).
[44]S. D. Pinches, L. C. Appel, J. Candy *et al.*, Comput. Phys. Commun. **111**, 133 (1998).
[45]D. Borba and W. Kerner, J. Comput. Phys. **153**, 101 (1999).
[46]T. E. Stringer, Plasmas Phys. **16**, 651 (1974).
[47]H. L. Berk, J. W. Van Dam, Z. Guo, and D. M. Lindberg, Phys. Fluids B **4**, 1806 (1992).

Downloaded 03 Oct 2012 to 194.81.223.66. Redistribution subject to AIP license or copyright; see http://pop.aip.org/about/rights_and_permissions